Variability of Passive Microwave Radiometric Signatures at Different Spatial Resolutions and Its Implication for Rainfall Estimation

Dong-Bin Shin, Kenneth P. Bowman, Jung-Moon Yoo, and Long S. Chiu, *Senior Member, IEEE*

***Abstract*—Analysis of precipitation radar (PR) and Tropical Rainfall Measuring Mission (TRMM) microwave imager (TMI) data collected from the TRMM satellite shows that rainfall inhomogeneity, as represented by the coefficient of variation (CV), depends on a spatial scale, i.e., the CV appears to be nearly constant at all rain rates within the field of view (FOV) of the TMI 37-GHz channel, while it decreases with rain rate at lower spatial resolutions, such as the FOV sizes of the low-frequency TMI channels (10.7 and 19.4 GHz). It is known that the brightness temperature $(T_{\rm b})$ for a low-frequency channel decreases with increasing rainfall inhomogeneity for a given rain rate. As such, more inhomogeneous rainfall at low rain rates leads to a lower $T_{\rm b}$ compared with that of a FOV with homogeneous rainfall; however, less inhomogeneous rainfall at high rain rates tends to produce a $T_{\rm b}$ similar to that of homogeneous rainfalls. These results indicate that the observed radiometric signatures of low-frequency channels at low spatial resolutions are characterized by a larger response range and smaller variability than those at a higher spatial resolution. Based on the observational characteristics of the TMI and PR data sets, we performed synthetic retrievals of rainfalls, employing a Bayesian retrieval methodology at different retrieval resolutions corresponding to the FOV sizes of the TMI channels at 10.7, 19.4, and 37 GHz. Comparisons of the rainfalls retrieved at the different resolutions and their temporal and regional averages show that the systematic bias resulting from the rainfall inhomogeneity is smaller in the lower resolution data than in their higher resolution counterparts. We note that such low-resolution rainfall retrievals are not expected to describe the instantaneous features of rain fields; however, they could be useful for climatological estimates at large temporal and spatial scales.**

***Index Terms*—Passive microwave remote sensing, precipitation, rainfall variability.**

I. Introduction

GLOBAL cloud and precipitation information has been collected by microwave, infrared, and visible sensors from low Earth orbiting and geostationary satellites. Considering that clouds are largely transparent to microwave radiation, microwave sensors can measure the thermal emission from rain within and below clouds, which allows for the direct estimation of the surface rain rate. In particular, frequencies below ~30 GHz are well suited for detecting rainfall over the ocean, where the emission from raindrops is clearly separated from the ocean surface emission by their different emissivities. The signals over land, however, are not as distinct, due to the high emissivity of land surfaces. On the other hand, scattering signatures at frequencies above ~50 GHz, indicated by the depression of radiance or brightness temperature due to frozen hydrometeors, are more effective in detecting rainfall over land. The scattering-based estimates, however, suffer from the indirect link between the frozen hydrometeor content at higher altitudes and the precipitation rate near the surface.

Early retrievals based on microwave emission estimated rainfall from observed radiances by using a simple 1-D cloud model [1]. The need for more realistic (3-D) cloud models in physically based retrieval algorithms was emphasized by a number of investigators (e.g., see [2]–[6]). Estimations based upon 3-D cloud models benefit from the simultaneous use of radiometric signatures from multiple-frequency channels, including both emission and scattering channels. Lower frequency channels have a larger response range in the radiometric signals as well as greater ability to penetrate into the rain layers than higher frequency channels. Microwave sensors on current satellites have relatively large fields of view (FOVs). Large FOVs can lead to the so-called "beam-filling" error, which occurs due to the combined effects of rainfall inhomogeneity within the sensor FOV and the nonlinear dependence of microwave brightness temperature $(T_{\rm b})$ on rain rate (R). This inherent problem can significantly decrease the response range and hamper the use of lower frequency channels to obtain accurate rain fields. Chiu *et al.* [7] presented an approximate formula for interpretation of the beam-filling error, as follows:

$$[R] - R_E \approx -\frac{1}{2}\left\{(R-[R])^2\,\frac{T_{\rm b}''([R])}{T_{\rm b}'([R])}\right\} \tag{1}$$

where R is the rain rate at the subpixel level; R_E is the estimated rain rate; $[R]$ is the true rain rate, with [ ] representing the FOV average; and $T_{\rm b}''$ and $T_{\rm b}'$ are the curvature and the slope of the $T_{\rm b}-R$ relation, respectively. In the case where the $T_{\rm b}-R$ relation is the exponential function

$$T_{\rm b}(R) = A - Be^{-CR} \tag{2}$$

Manuscript received April 4, 2008; revised July 30, 2008. First published December 2, 2008; current version published May 22, 2009. This work was supported in part by the Korea Research Foundation program under Grant KRF-2007-314-C00306 and in part by Yonsei University under Grant 2007-7-0179.

D.-B. Shin is with the Department of Atmospheric Sciences, Yonsei University, Seoul 120-749, Korea (e-mail: dbshin@yonsei.ac.kr).

K. P. Bowman is with the Department of Atmospheric Sciences, Texas A&M University, College Station, TX 77843 USA.

J.-M. Yoo is with the Department of Science Education, Ewha Womans University, Seoul 120-750, Korea.

L. S. Chiu is with the Institute of Space and Earth Information Science, Chinese University of Hong Kong, Shatin, Hong Kong.

Color versions of one or more of the figures in this paper are available online at http://ieeexplore.ieee.org.

Digital Object Identifier 10.1109/TGRS.2008.2007740

where A, B, and C are adjustable parameters; we can get $T_{\rm b}''/T_{\rm b}' = -C$. Note that the variance of rain rate with respect to the averaging area $(R-[R])^2$ and the parameter C are positive; hence, the right-hand side of (1) is greater than zero. Therefore, statistically, the estimated rain rate is less than the true rain rate (a negative bias). Some studies, such as Short and North [8] and Ha and North [9], suggest that better estimated rain rates can be obtained by using a constant multiplicative factor. Wang [10] examined the slant path attenuation for various hydrometeor distributions and proposed that the beam-filling correction factor is not a constant factor but that it is linearly related to the freezing height (rain-column height). Wang [10] also argued that convective rains are associated with a higher freezing height and a higher rain rate variance. This is consistent with the notion that a higher rain rate variance is associated with convective rain than stratiform rain; hence, a higher beam-filling correction is required.

If we divide both sides of (1) by $[R]$, we get

$$\begin{aligned}([R]-R_E)/[R] &\approx -\frac{1}{2}\left\{(R-[R])^2/[R]^2\frac{T_{\rm b}''([R])}{T_{\rm b}'([R])}\right\}[R] \\ &\approx -\frac{1}{2}\left\{{\rm CV}^2\frac{T_{\rm b}''([R])}{T_{\rm b}'([R])}\right\}[R] \qquad (3)\end{aligned}$$

where CV is the coefficient of variation which can be obtained by dividing the standard deviation (SD) of rainfall by $[R]$. The left-hand side is the percent error due to the beam-filling error. This formula states that the percent error due to the beam-filling error is proportional to the square of the CV and, linearly, to $[R]$. Nzeukou *et al.* [11] examined rain rate statistics from ground radar observations and suggested that CV is relatively constant over many cities. In this case, the percent error due to beam filling is then linearly related to the mean rain rate, i.e., the higher the rain rate, the larger the beam-filling error.

The Tropical Rainfall Measuring Mission (TRMM) spaceborne precipitation radar (PR) provides rain rates at a 4-km resolution. This paper uses PR data to check the relationship between CV and $[R]$ for different rain regimes and at different temporal scales. Previous studies were mainly concerned about reducing or measuring the beam-filling error that occurred from the use of the brightness temperature $(T_{\rm b})$ relations to homogeneous rainfalls in retrievals. However, this paper investigates the microwave radiometric responses associated with the rainfall inhomogeneity at different retrieval resolutions and their impacts on rainfall estimations.

II. Data

The TRMM microwave imager (TMI) measures upwelling microwave radiances (brightness temperatures) emitted by the Earth and atmosphere at five frequencies, namely, 10.7, 19.4, 21.3, 37.0, and 85.5 GHz, with both horizontal and vertical polarizations (only vertical polarization at 21.3 GHz). The radiometer views the atmosphere at an oblique angle (49°) corresponding to an Earth incidence angle of 52.8°. The swath width of the TMI is 758.5 km. At each frequency, the instantaneous FOV (IFOV) is determined by the satellite altitude, viewing angle, antenna size, and beam width. Considering that the TMI antenna rotates while its receiver is integrating, the effective area scanned by the antenna beam is different from IFOV. The effective area is called the effective FOV (EFOV). The standard TMI brightness temperature data are provided at the EFOV level; however, for the lower frequency channels, the data are provided at the level of the beam EFOV that combines a specific number of the EFOVs in the cross-track direction. The beam EFOV at 10.7 GHz is 63 × 37 km (down- and cross-track directions). At frequencies of 19.4, 21.3, 37.0, and 85.5 GHz, the FOVs are 30 × 18, 23 × 18, 16 × 9, and 7 × 5 km, respectively. The TMI data at the beam EFOV level are used in this paper. The TRMM PR operates at 13.8 GHz and measures the return power with a range resolution of 250 m for normal samples, a nadir resolution of ∼4 km, and a swath width of 215 km. The reflectivity profiles are converted to rain rate profiles using a reflectivity–rain rate $(Z-R)$ relationship developed by Iguchi *et al.* [12]. Precipitation types classified as stratiform, convective, and other are also provided. The details of the TRMM instruments and algorithms can be found in [13].

This paper uses the version 6 TMI brightness temperatures (TRMM product number 1B11) and PR data (2A23 and 2A25) acquired from the National Aeronautics and Space Administration/Goddard Space Flight Center Distributed Active Archive Center. The PR rainfall data are averaged over the three resolutions corresponding to the FOVs of the TMI's 10.7-, 19.4-, and 37.0-GHz channels. Analyses are carried out over sections of the eastern Pacific $(0^\circ\ {\rm N}{-}15^\circ\ {\rm N}, 130^\circ\ {\rm W}{-}100^\circ\ {\rm W})$ and western Pacific $(0^\circ\ {\rm N}{-}15^\circ\ {\rm N}, 135.5^\circ\ {\rm E}{-}165.5^\circ\ {\rm E})$ during the period of December 1999–February 2000 (DJF, 1999–2000).

III. Characteristics of Rainfall Inhomogeneity

A. Different Spatial Resolutions

The spatial inhomogeneity of a rain field for a given area may be described by the CV, which is defined as the ratio of the SD to mean. This paper uses the spatial information from PR near surface rainfalls. The CV of rainfall within a FOV is computed as

$${\rm CV} = \left\{\frac{1}{N}\sum_{i=1}^{N}(R_i-[R])^2\right\}^{0.5}\Big/[R] \qquad (4)$$

where R indicates the PR near surface rainfall at the resolution of ∼4 km and its average within a FOV is represented by square brackets. N indicates the number of PR pixels within the FOV.

Fig. 1 shows the variation of CV as a function of the FOV-averaged PR rain rate for the eastern and western Pacific during the DJF period of 1999–2000 at the resolutions of the 37.0-, 19.4-, and 10.7-GHz TMI channels. The FOVs of the three channels are abbreviated by $\rm FOV_{37}$, $\rm FOV_{19}$, and $\rm FOV_{10}$ representing 16 × 9, 30 × 18, and 63 × 37 km, respectively. There is an interesting feature in the behavior of the rainfall inhomogeneity depending on the spatial resolution. At the resolution of $\rm FOV_{37}$, the CV is relatively constant, implying that the SD is linearly related to the mean rain rate. At the lower resolutions, however, CV decreases as a function of rain rate, showing that lower rain rates are more variable (less homogeneous) but that higher rain rates are less variable (more homogeneous) at the higher resolution than at the lower resolution.

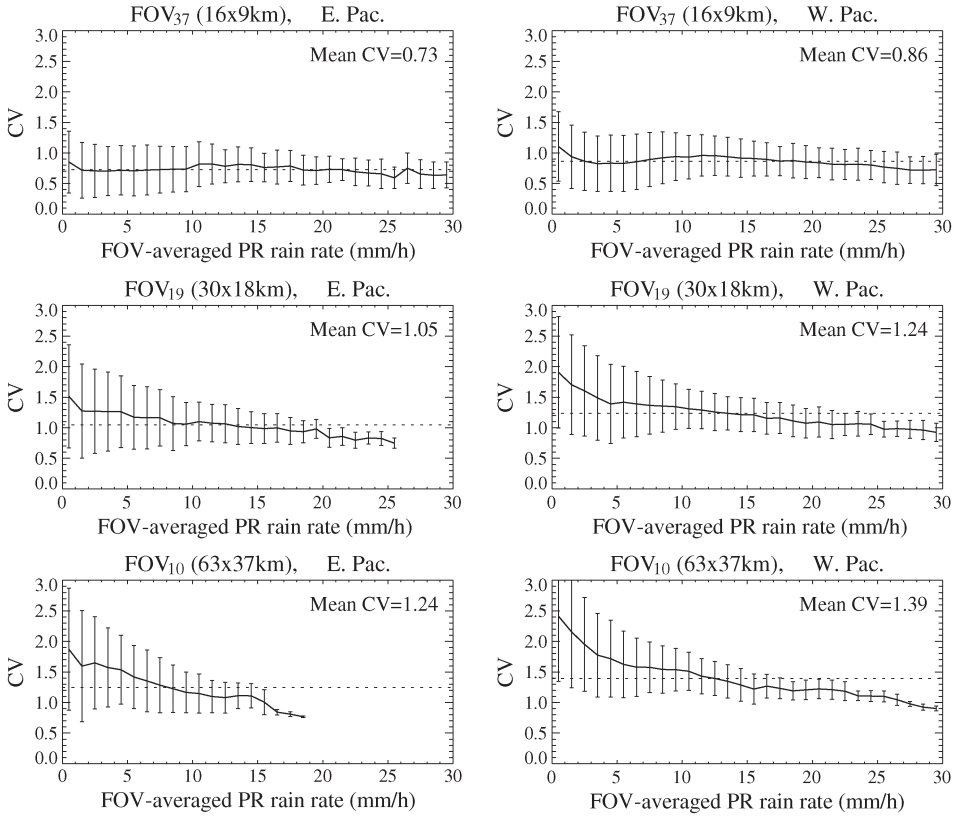

Fig. 1. CV as a function of the FOV-averaged PR rain rate at three different resolutions FOV_{37} (16 × 9 km), FOV_{19} (30 × 18 km), and FOV_{10} (63 × 37 km) for the eastern and western Pacific. Each dotted line indicates the average of CVs at all rain intensities. The error bars represent the ±1 SDs.

We can also see that the average CVs, indicated by the dotted lines, increase with FOV size and are 0.73, 1.05, and 1.24 at FOV_{37}, FOV_{19}, and FOV_{10}, respectively, for the eastern Pacific and 0.86, 1.24, and 1.39 for the western Pacific. The CV for the western Pacific is also consistently higher than that for the eastern Pacific for the same FOVs. The different rainfall variabilities in different regions are also discussed in the previous work by Kummerow *et al.* [14].

In Fig. 2, histograms of PR rain rates are shown, grouped by three different categories of CV for the three different FOV sizes. The three groups of CV are defined by $\mathrm{CV_L}$ for $\mathrm{CV} < 1$, $\mathrm{CV_M}$ for $1 \leq \mathrm{CV} < 2$, and $\mathrm{CV_H}$ for $2 \leq \mathrm{CV}$, where the subscripts, L, M, and H denote low, medium, and high in the rainfall inhomogeneity, respectively. In general, the curves in Fig. 2 show monotonic decreases on a logarithmic scale, suggesting a Gamma or lognormal distribution. It is known that tropical rainfalls are well fitted by the lognormal or gamma distributions [15], and the results shown in Fig. 2 support that observation. There are also several features in the rainfall distributions that occur commonly in the eastern and western Pacific. At the smallest area (FOV_{37}) among the tested FOVs, (solid line) rainfall with low rainfall inhomogeneity $\mathrm{CV_L}$ is observed more frequently than rainfall with medium and high rainfall variabilities ($\mathrm{CV_M}$ and $\mathrm{CV_H}$), indicated by dotted and dashed lines, respectively. As the FOV size increases, however, a greater occurrence of rainfall in the $\mathrm{CV_M}$ and $\mathrm{CV_H}$ categories is observed. The other highlight is that rainfall within the $\mathrm{CV_H}$ category has a narrower range of distribution, ending at ∼10 mm/h for the eastern Pacific and ∼15 mm/h for the western Pacific. This may indicate that the higher rain rates are usually accompanied by low or medium rainfall inhomogeneity.

B. Stratiform and Convective Precipitation

We next classify the rainfall data by the CV and the fraction of convective precipitation at the resolution of the 19.4-GHz channel (FOV_{19}). The convective fraction at FOV_{19} is defined as the ratio of the number of pixels (4 km) classified as convective rain to the total number of raining pixels. The classification of the rain types is obtained from the TRMM product 2A23. Fig. 3 shows the relationships between the rain rate (R) and CV for two different fractions of convective rain at FOV_{19}. The first case, indicated by a solid line, represents the $\mathrm{CV}-R$ relationship when the raining pixels in FOV_{19} have no convective rain, and the (dotted line) second case represents the $\mathrm{CV}-R$ relationship when more than 50% of raining pixels in the FOV have convective rain. The separation of the two different cases by CV, as well as rain rate, is very apparent, i.e., the first case, which has no convective pixels, appears to be associated with lower CV and lower rain rates than the second case, which has more convective pixels, suggesting a relationship between the horizontal rainfall inhomogeneity and the vertical rain structure. It seems that nonconvective (stratiform) and highly convective rains are roughly divided by the line $\mathrm{CV} \approx 0.9$ for the eastern Pacific and $\mathrm{CV} \approx 1.1$ for the western Pacific. The values of CV presented here for discriminating the two cases may be appropriate only for the season and regions used in this paper. Different seasons and

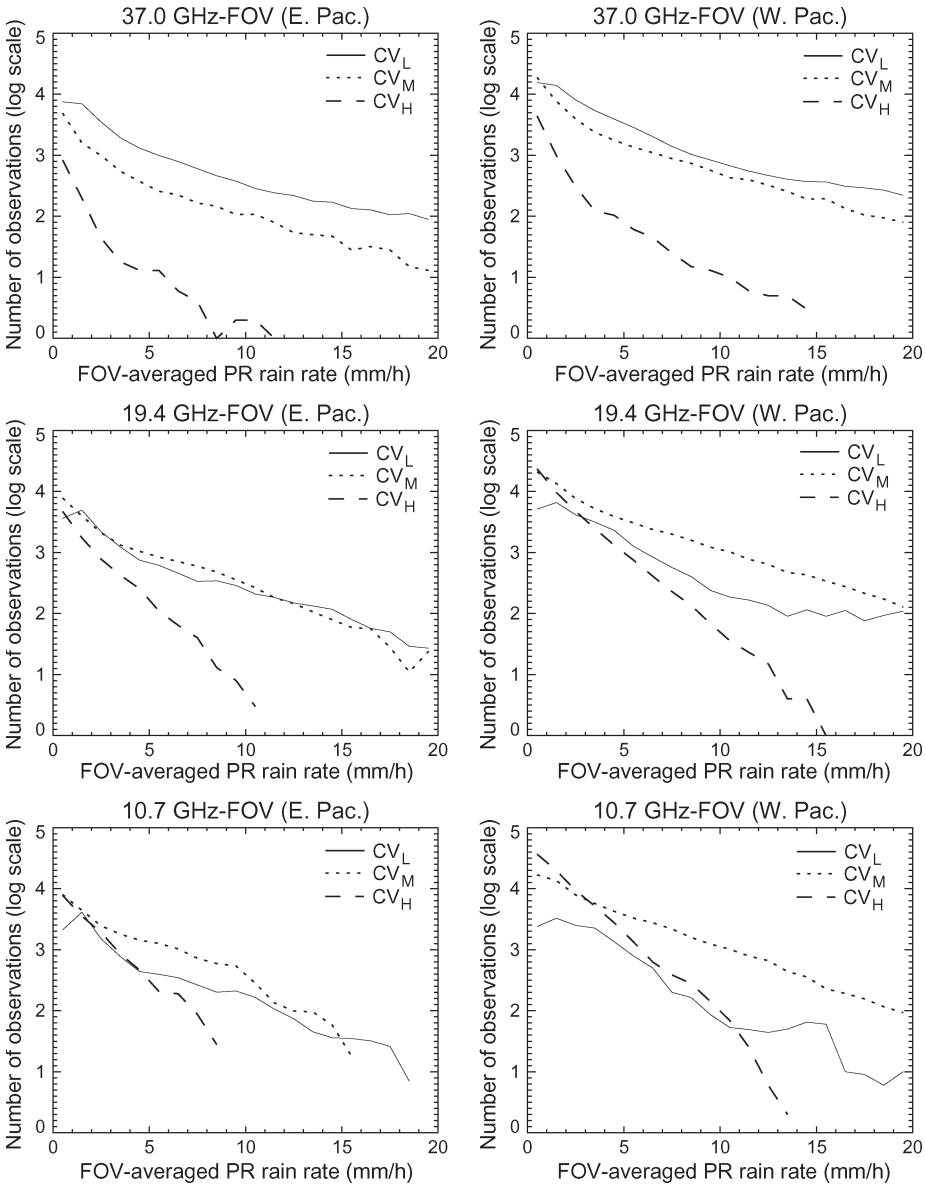

Fig. 2. Histograms of FOV-averaged PR rain rate at FOV_{37}, FOV_{19}, and FOV_{10} for three different CVs over the eastern and western Pacific.

regions could have different values of the CV. As shown in Fig. 4, the (solid line) $\mathrm{CV}-R$ relationship for cases that have less than 50% convective rain pixels is compared with the (dotted line) relationship from the case where more than 50% of the pixels are convective rain. Note that the curve for the case with the higher convective fraction is already shown in Fig. 3 but is repeated here for comparison. Fig. 4 simply shows that the two cases with different convective fractions in the FOV are indistinguishable, although the case with the higher convective fraction is not observed for lower rain rates.

IV. Radiometric Signatures at Different Spatial Resolutions

The radiometric signatures of the low-frequency TMI channels are mostly determined by the emission properties of hydrometeors along the path, due to the transmissivity of clouds at these wavelengths. The measured brightness temperatures are determined by both the amounts and distributions of the hydrometeors. The combined effect of spatially inhomogeneous rainfall and coarse resolutions of the low-frequency channels contributes to inhomogeneity on the emission signatures, resulting in an ambiguity in rainfall retrievals. This section investigates how the radiometric signatures vary as a function of the spatial inhomogeneity of rainfall and the different spatial resolutions.

Fig. 5 shows the observed $T_{\mathrm{b}}-R$ relationships at 10.7 GHz-H (horizontal polarization) and 19.4 GHz-H as a function of CV for the eastern and western Pacific during the DJF period of 1999–2000. The means that the curves grouped by the three different rainfall inhomogeneity parameters, $\mathrm{CV_L}$, $\mathrm{CV_M}$, and $\mathrm{CV_H}$ (low, medium, and high variabilities, respectively), indicated by black dots, appear to be well separated. As inferred from the mean curves, a brightness temperature can be associated with different rain rates depending on the rainfall inhomogeneity. This nonuniqueness in the $T_{\mathrm{b}}-R$ relationship resulting

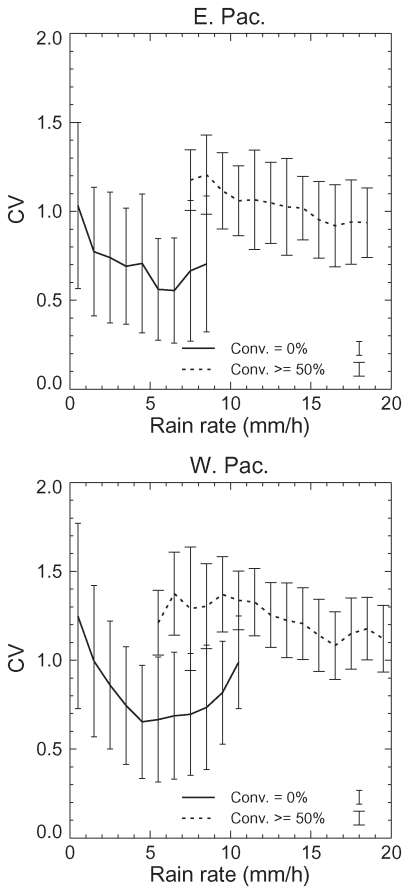

Fig. 3. Relationships between rainfall and CV for two different fractions of convective precipitation at the resolution of 19.4-GHz channel ($\mathrm{FOV}_{19} = 30 \times 18$ km). The error bars show the ± 1 SDs as before.

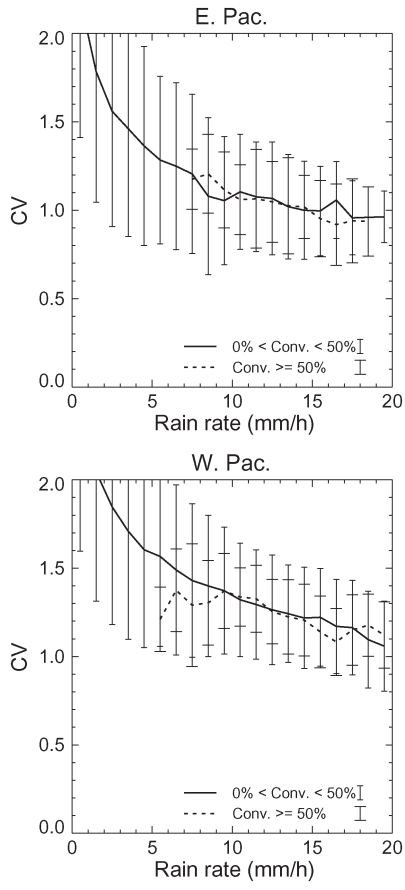

Fig. 4. Same as Fig. 3 but for the two cases that (dotted line) more than and (solid line) less than 50% of raining pixels in the FOV are convective rainfalls.

from the inhomogeneity of rainfall causes the beam-filling error in retrievals. The mean curves simply indicate that the beam-filling bias increases with increasing CV and rainfall intensity. The ± 1 SD error bars of T_b and the (the dotted lines) median T_b are also presented to show the dispersion and symmetry of the T_b distribution at each rain interval, respectively. The mean and median of the T_bs are close, suggesting that the T_b's grouped by the same CV class and the same rain intensity tend to have a symmetrical distribution (not shown here but is roughly a normal distribution). It is also shown that the error bars for the case of CV_M are overlapped with the adjacent CV_L and CV_H, whereas those for the low CV_L and high CV_H CVs appear to be well separated.

As reviewed in Section III-A, there is a distinct behavior of the rainfall inhomogeneity depending on rain rates and spatial resolutions, i.e., at the lower resolutions (FOV_{10} and FOV_{19}), low rain rates occur less homogeneously than high rain rates, whereas at the higher resolution (FOV_{37}), the rainfall inhomogeneities are similar at both low and high rain rates. As can be inferred from (1), for a given rain rate, T_b tends to decrease as the rainfall inhomogeneity increases. The different distributions of the rainfall inhomogeneity with varying spatial resolutions can then affect the $T_\mathrm{b}-R$ relationships. Fig. 6 shows the $T_\mathrm{b}-R$ relationships at the higher and lower spatial resolutions (FOV_{37} and FOV_{10}) for the eastern and western Pacific. The $T_\mathrm{b}-R$ relationships at 10.7 GHz-H for the two resolutions are shown in the upper panels [Fig. 6(a) and (b)]. The rainfall data at the PR pixels ($\sim$4 km) are averaged over the two FOVs. The T_b data from the 10.7 GHz channel encompassing the two FOVs are used to represent the 10-GHz T_b data at the resolutions of FOV_{10} and FOV_{37}, respectively. In obtaining the 10.7-GHz T_b data at the resolution of FOV_{37}, the 10-GHz T_b data at every fourth pixels of the 37.0-GHz FOV are selected to avoid sampling of overlapped 10.7-GHz T_b data. The 19-GHz T_b's at the 37-GHz resolution are obtained similarly. For both regions, it can be seen that the T_b's at FOV_{10} are slightly lower than those at FOV_{37} for lower rain rates (below 3–4 mm/h) but are higher at larger rain rates, i.e., lower rain rates are associated with the greater values of rainfall inhomogeneity (Fig. 1), resulting in lower T_b at the lower resolution (FOV_{10}) than at the higher resolution (FOV_{37}). This situation is reversed as the rain rate increases because emissions from more homogenous rainfall at the lower resolution (FOV_{10}) contribute to the warmer T_b. If homogeneous rainfall is involved, the two FOVs should have equivalent T_b's. As such, it seems that the actual distribution of the rainfall inhomogeneity contributes to a greater range of T_b responses at FOV_{10} than at FOV_{37}. The lower panels represent the relationships between 19-GHz-H T_b and R at the same resolutions [Fig. 6(c) and (d)] and demonstrate similar results. We can also see that the variability of the T_b's, as indicated by the error bars, is smaller for the larger FOV. The $T_\mathrm{b}-R$ relations over the FOV_{19} (not shown) are located between those for the FOV_{37} and FOV_{10} resolutions.

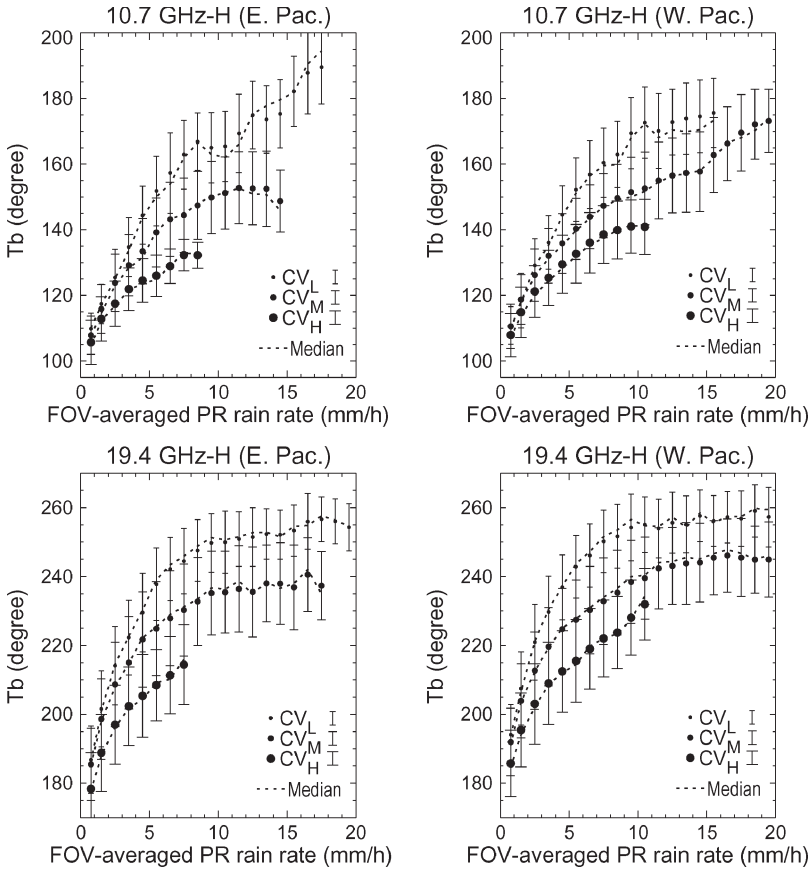

Fig. 5. Mean relationship between TMI brightness temperature ($T_{\rm b}$) and PR surface rain rate, indicated by black dots, at 10.7- and 19.4-GHz horizontally polarized channels for three different categories of the rainfall inhomogeneities $\mathrm{CV_L}$, $\mathrm{CV_M}$, and $\mathrm{CV_H}$ (low, medium, and high inhomogeneities, respectively) over the eastern and western Pacific. The median $T_{\rm b}$'s are shown in dotted lines. The error bars show the ± 1 SDs as before.

In physically based rainfall algorithms, the desired inference depends heavily upon the prior knowledge of the radiometric response. For this reason, when cloud–radiative transfer model simulations are used to establish *a priori* information, it is important to have the prior information as close to nature as possible to better represent the precipitation fields. The decreasing response ranges resulting from the use of lower resolution $T_{\rm b}$ at higher resolutions, as shown by the $T_{\rm b}-R$ relations in Fig. 6, can cause the uncertainty in retrieval processes. The uncertainty then may be considered as an inherent error that cannot be solved by improving *a priori* information from better cloud–radiative transfer models. Such better models would reduce only the differences between the simulated and observed fields; however, the uncertainties in the radiometric signatures due to the nature of precipitation variability remain intact. On the other hand, the radiometric signatures from the lower resolution channels convolved at the lower resolution (FOV_{10}) are characterized by the larger response range and smaller variability than at the higher resolution (FOV_{37}). It may imply that the low-resolution rainfall estimates can have less systematic bias than the high-resolution estimates if the actual rainfall distribution is well maintained in retrievals. The low-resolution rainfall retrievals are not capable of describing the details of instantaneous rainfall rates. The smaller bias can be used, however, to obtain better climatological estimates. In order to demonstrate this effect, we will perform synthetic rainfall retrievals at different retrieval resolutions based on the observed $T_{\rm b}$ and rainfall databases in the next section.

V. Synthetic Retrievals

A. Retrieval Method

Our retrieval algorithm, which is used to estimate rainfall at different retrieval resolutions, does not include any complicated procedures to increase the retrieval performance; however, a straightforward Bayesian inversion method is employed. The *a priori* databases for the retrieval are computed separately by averaging the rainfall and $T_{\rm b}$'s of each channel over the retrieval resolutions, as shown in Fig. 6. Once a database is generated, the inversion problem is resolved by the Bayesian methodology, as used by Shin and Kummerow [16]. Similar Bayesian methodologies have been used previously (e.g., [6], [17], and [18]). In this approach, the state vector $\mathbf{h}$ can be PR rain parameters and the measurement vector $\mathbf{b}$ will be the set of TMI brightness temperatures. The posterior probability, which is the object of the Bayesian inference, may be expressed as

$$P(\mathbf{h} \mid \mathbf{b}) \propto P(\mathbf{b} \mid \mathbf{h}) P(\mathbf{h}) \tag{5}$$

where $P(\mathbf{b}|\mathbf{h})$ is the probability of $\mathbf{h}$ conditional on $\mathbf{b}$. As outlined by Rodgers [19], the conditional probability $P(\mathbf{b}|\mathbf{h})$ may be modeled by a multidimensional Gaussian distribution

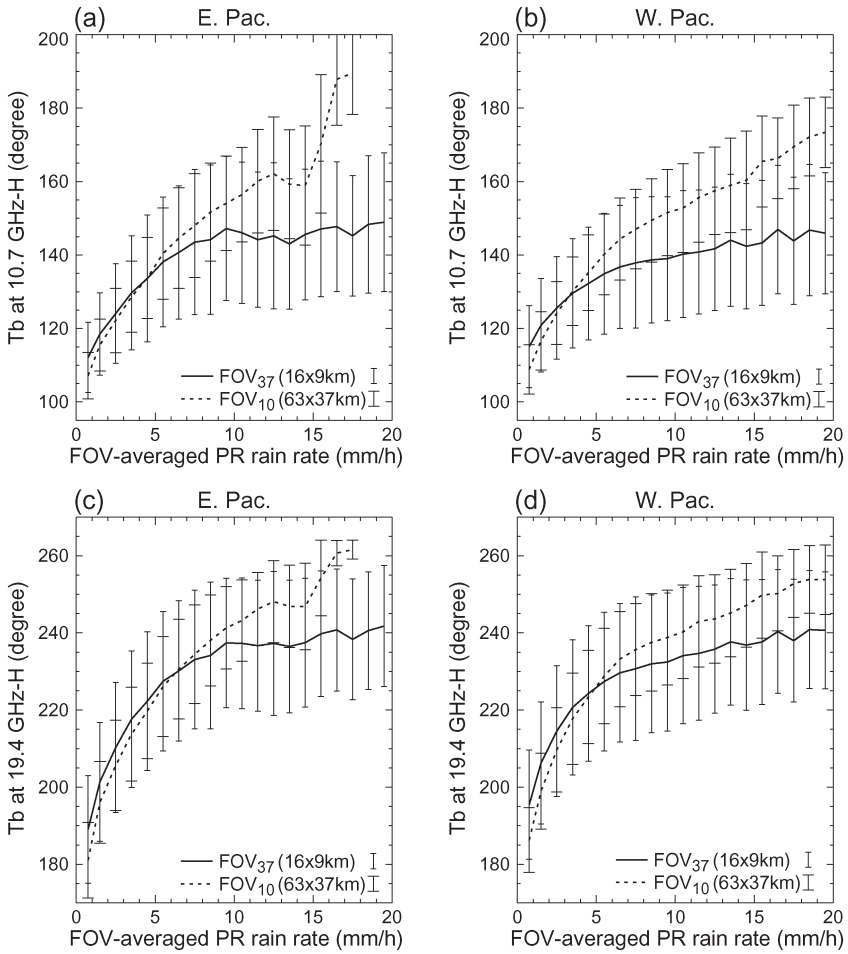

Fig. 6. Relationships between $T_{\rm b}$ and R obtained at two different spatial resolutions (solid line) FOV_{37} and (dotted line) FOV_{10} over the eastern and western Pacific. The 10.7-GHz-H $T_{\rm b}$ to R relation is shown in the upper panels, and the lower panels represent the 19.4-GHz-H $T_{\rm b}$ to R relations. The error bars denote the ± 1 SDs as before.

of the difference between the observation and the modeled observation, with the uncertainty given by the measurement and forward simulation. In a retrieval using the observational database, the error from the forward computations will not appear in the covariance matrix for the term $P(\mathbf{b}|\mathbf{h})$. The covariance matrix has only the diagonal elements of the instrumental noises at each channel. The synthetic retrievals are intended to compare the rainfall estimates at different retrieval resolutions such that the PR data are averaged over the retrieval resolutions. Furthermore, since $P(\mathbf{h})$ of the prior information is a good description of the true probability distribution of precipitation fields, $P(\mathbf{h})$ is simply replaced by the frequency of each element in the prior information, i.e., we assume that the database created from three months of TRMM data represents the distribution and variability of rain profiles well.

B. Comparison of Retrieved Rainfall

The comparison of the rainfall retrieved at the three different retrieval resolutions FOV_{37}, FOV_{19}, and FOV_{10} over the eastern Pacific during DJF, 1999-2000 is shown in Fig. 7. The bias, rms error, and correlation between the PR and estimate rainfalls are consistently improved at lower frequency resolutions due to the larger response range and reduced variability in the $T_{\rm b}-R$ relationship. However, the direct comparison of the retrieval results for different resolutions is not appropriate because the high-resolution retrieval itself has great benefits for observing the details of precipitation. Moreover, some important constraining information that can increase the retrieval performance significantly is not considered in the retrievals. As such, the comparison of the estimates from the different resolutions is not of interest in this paper. These results only emphasize that accurate low-resolution estimates can be achieved if the appropriate information on $T_{\rm b}$ and R relations for the retrieval resolution is used.

We next compare the rainfall estimates at the resolution of FOV_{10}. In the averaging of the higher resolution estimates into FOV_{10}, about 16 pixels of FOV_{37} and about four pixels of FOV_{19}, which correspond approximately to the size of FOV_{10}, are involved. The retrieval statistics averaged from the higher resolutions FOV_{37} and FOV_{19} to FOV_{10} are shown in rows (a) and (b) of Table I, respectively. The statistics corresponding to rainfall directly estimated at FOV_{10}, as already shown in Fig. 6(c), are also presented in row (c) for comparison. As expected, averaging higher resolution estimates at FOV_{37} or FOV_{19} over the lower resolution pixels FOV_{10} does not change the bias statistics but decreases the rms error and increases the correlation (refer to the numbers shown in Fig. 6(a) and (b)

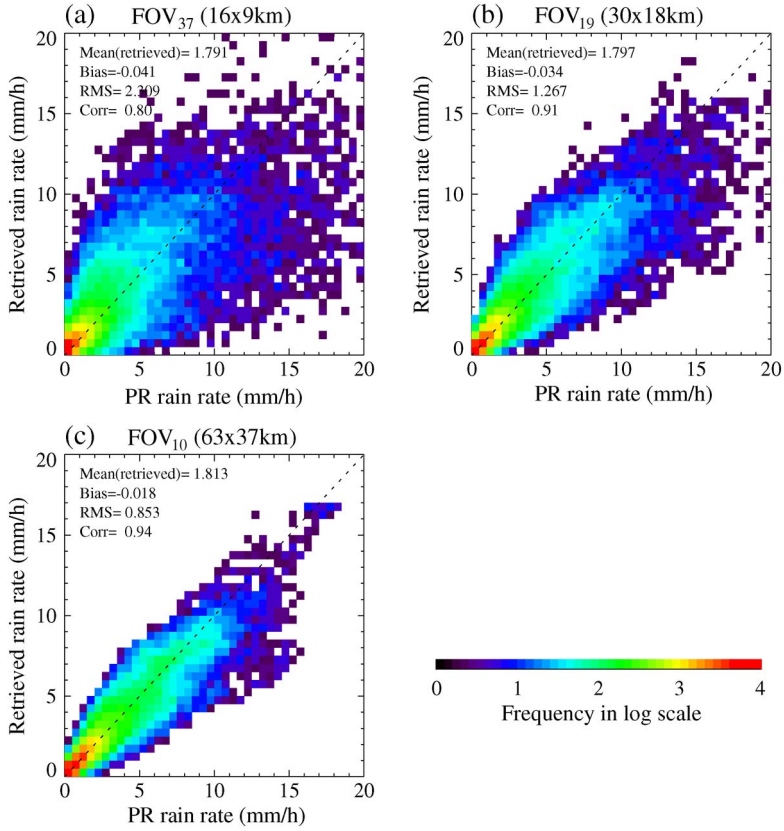

Fig. 7. Two-dimensional histograms showing the PR and estimated rain rates at different resolutions of 37.0-, 19.4-, and 10.7-GHz channels. Synthetic retrievals are performed over the eastern Pacific during the period of DJF, 1999–2000. Color in square box indicates frequency in log scale.

TABLE I
STATISTICS OF THE RAINFALL ESTIMATES AT THE RESOLUTION OF FOV_{10} FOR THE EASTERN PACIFIC. THE RAINFALLS AT FOV_{37} AND FOV_{19} ARE AVERAGED OVER THE RESOLUTION OF FOV_{10} AND ARE PRESENTED IN ROWS (a) AND (b), RESPECTIVELY. ROW (c) ALSO SHOWS THE STATISTICS OF ESTIMATES DIRECTLY PERFORMED AT FOV_{10}. NUMBERS IN PARENTHESES REPRESENT PERCENT VALUE OF THE PR MEAN RAIN RATE

	Mean rain rate				
	PR	Estimated	Bias	RMS	Correlation
(a) Averaged from FOV_{37}	1.832	1.791	-0.041 (-2.237%)	1.194	0.89
(b) Averaged from FOV_{19}	1.832	1.798	-0.034 (-1.871%)	1.129	0.92
(c) FOV_{10}	1.832	1.813	-0.018 (-1.005%)	0.853	0.94

TABLE II
SAME AS TABLE I BUT FOR THE WESTERN PACIFIC

	Mean rain rate				
	PR	Estimated	Bias	RMS	Correlation
(a) Averaged from FOV_{37}	1.894	1.871	-0.023 (-1.215%)	1.271	0.84
(b) Averaged from FOV_{19}	1.894	1.880	-0.014 (-1.744%)	1.332	0.88
(c) FOV_{10}	1.894	1.885	-0.010 (-0.508%)	1.185	0.90

for the corresponding high-resolution estimates). Meanwhile, the advantage of low-resolution retrievals directly performed at the low resolution is indicated by the better retrieval statistics resulting from the use of the *a priori* database that is characterized by the higher degree of linearity and greater ranges in the T_b responses to rain rates at the larger spatial scale. Similar results are found for the western Pacific (Table II).

VI. CONCLUSION

Analyses of TRMM PR observations show distinctive properties of the distributions of the rainfall inhomogeneity, represented by CV, depending on spatial resolution. Low rain rates have greater rainfall inhomogeneity at lower resolutions (FOV_{19} and FOV_{10}) than at higher resolutions (FOV_{37}), whereas higher rain rates seem to be associated with lower rainfall inhomogeneity. These results suggest that less homogeneous rainfall at low rain rates leads to lower T_b's; however, more homogeneous rainfall at high rain rates produces higher T_b's at lower resolutions than at higher resolutions. This effect is verified by the distributions of T_b's from each TMI emission channel, which are obtained at the different spatial resolutions. It also suggests that the rainfall inhomogeneity associated with a retrieval resolution may be an important

parameter to consider in building the relationships between $T_{\rm b}$ and R that are the basis of the physically based rainfall algorithms.

Considering that the radiometric signatures at the lower frequencies tend to maintain a greater response range than at the higher frequencies, which results from the different distribution of rainfall inhomogeneity with rain rates, this paper has introduced the possibility of using the low-resolution retrievals for the climatological estimates. Instantaneous rainfall estimates based on the observed TRMM information are retrieved at the three resolutions (FOV_{37}, FOV_{19}, and FOV_{10}) over the eastern and western Pacific during the period of DJF, 1999–2000. Low-resolution low-frequency estimates are shown to have a smaller bias than the high-resolution estimates (Fig. 7), mainly due to the greater range of $T_{\rm b}$ responses at the lower resolution. The smaller bias in the low-resolution estimates is still maintained when they are compared with the estimates obtained by averaging high-resolution rainfall over FOV_{10} (Tables I and II). It suggests that rainfall retrievals at lower resolutions (lower frequency) may produce better climatological estimates if the prior information (database) for retrievals contains appropriate $T_{\rm b}$ relations to R for the retrieval resolution. The regional and temporal variation of the rainfall inhomogeneity and its impact on the radiometric signatures to rainfall structures must still be investigated. The successful operation of the TRMM satellite for almost a decade will allow us to construct reliable information for a wide range of climatological conditions. The information can serve as the basis for the construction of the $T_{\rm b}$ relations to R, as well as for a comprehensive error model in passive microwave rainfall retrievals.

REFERENCES

[1] T. T. Wilheit, A. T. C. Chang, and L. S. Chiu, "Retrieval of monthly rainfall indices from microwave radiometric measurement using probability distribution functions," *J. Atmos. Ocean. Technol.*, vol. 8, no. 1, pp. 118–136, Feb. 1991.

[2] E. A. Smith and A. Mugnai, "Radiative transfer to space through a precipitating cloud at multiple microwave frequencies. Part II: Results and analysis," *J. Appl. Meteorol.*, vol. 27, no. 9, pp. 1074–1091, Sep. 1988.

[3] R. F. Adler, H.-Y. M. Yeh, N. Prasad, W.-K. Tao, and J. Simpson, "Microwave simulations of a tropical rainfall system with a three-dimensional cloud model," *J. Appl. Meteorol.*, vol. 30, no. 7, pp. 924–953, Jul. 1991.

[4] E. A. Smith, H. J. Cooper, X. Xiang, A. Mugnai, and G. Tripoli, "Foundations for statistical–physical precipitation retrieval from passive microwave satellite measurements. Part I: Brightness-temperature properties of a time-dependent cloud-radiation model," *J. Appl. Meteorol.*, vol. 31, no. 6, pp. 506–531, Jun. 1992.

[5] A. Mugnai, E. A. Smith, and G. J. Tripoli, "Foundations for statistical–physical precipitation retrieval from passive microwave satellite measurements. Part II: Emission-source and generalized weighting-function properties of a time-dependent cloud-radiation model," *J. Appl. Meteorol.*, vol. 32, no. 1, pp. 17–39, Jan. 1993.

[6] W. S. Olson, C. Kummerow, G. M. Heymsfield, and L. Giglio, "A method for combined passive–active microwave retrievals of cloud and precipitation profiles," *J. Appl. Meteorol.*, vol. 38, no. 10, pp. 1763–1789, Oct. 1996.

[7] L. S. Chiu, G. R. North, D. A. Short, and A. McConnell, "Rain estimation from satellites: Effect of finite field of view," *J. Geophys. Res.*, vol. 28, no. D3, pp. 2177–2185, Feb. 1990.

[8] D. A. Short and G. R. North, "The beam filling error in ESMR-5 observations of GATE rainfall," *J. Geophys. Res.*, vol. 95, no. D3, pp. 2187–2194, Feb. 1990.

[9] E. Ha and G. R. North, "Model studies of the beam-filling error for rain-rate retrieval with microwave radiometers," *J. Atmos. Ocean. Technol.*, vol. 12, no. 2, pp. 268–281, Apr. 1995.

[10] S. A. Wang, "Modeling the beamfilling correction for microwave retrieval of oceanic rainfall," Ph.D. dissertation, Texas A&M Univ., College Station, TX, 1996.

[11] A. Nzeukou, H. Sauvageot, A. D. Ochou, and C. M. F. Kebe, "Raindrop size distribution and radar parameters at Cape Verde," *J. Appl. Meteorol.*, vol. 43, no. 1, pp. 90–105, Jan. 2004.

[12] T. Iguchi, T. Kozu, R. Meneghini, J. Awaka, and K. Okamoto, "Rain-profiling algorithm for the TRMM Precipitation Radar," *J. Appl. Meteorol.*, vol. 39, no. 12, pp. 2038–2052, Dec. 2000.

[13] C. Kummerow, W. Barnes, T. Kozu, J. Shiue, and J. Simpson, "The Tropical Rainfall Measuring Mission (TRMM) sensor package," *J. Atmos. Ocean. Technol.*, vol. 15, no. 3, pp. 809–817, Jun. 1998.

[14] C. Kummerow, P. Poyner, W. Berg, and J. Thomas-Stahle, "The effects of rainfall inhomogeneity on climate variability of rainfall estimated from passive microwave sensors," *J. Atmos. Ocean. Technol.*, vol. 21, no. 4, pp. 624–638, Apr. 2004.

[15] H. K. Cho, K. P. Bowman, and G. R. North, "A comparison of gamma and lognormal distributions for characterizing satellite rain rates from the Tropical Rainfall Measuring Mission," *J. Appl. Meteorol.*, vol. 43, no. 11, pp. 1586–1597, Oct. 2003.

[16] D.-B. Shin and C. Kummerow, "Parametric rainfall retrieval algorithms for passive microwave radiometers," *J. Appl. Meteorol.*, vol. 42, no. 10, pp. 1480–1496, Oct. 2003.

[17] C. Kummerow, W. S. Olson, and L. Giglio, "A simplified scheme for obtaining precipitation and vertical hydrometeor profiles from passive microwave sensors," *IEEE Trans. Geosci. Remote Sens.*, vol. 34, no. 5, pp. 1213–1232, Sep. 1996.

[18] F. S. Marzano, A. Mugnai, G. Panegrossi, N. Pierdicca, E. A. Smith, and J. Turk, "Bayesian estimation of precipitating cloud parameters from combined measurements of spaceborne microwave radiometer and radar," *IEEE Trans. Geosci. Remote Sens.*, vol. 37, no. 1, pp. 596–613, Jan. 1999.

[19] C. D. Rodgers, *Inverse Methods for Atmospheric Sounding: Theory and Practice*. Singapore: World Scientific, 2000, ch. 3.

Dong-Bin Shin received the B.S. and M.S. degrees in meteorology from Yonsei University, Seoul, Korea, in 1987 and 1989, respectively, and the Ph.D. degree in atmospheric sciences from Texas A&M University, College Station, in 1999.

He was a Research Professor with the Center for Earth Observing and Space Research, School of Computational Sciences, George Mason University, Fairfax, VA, and was also with the Department of Atmospheric Science, Colorado State University, Fort Collins, as a Research associate. He is currently an Associate Professor with the Department of Atmospheric Science, Yonsei University. His research interests include satellite remote sensing of clouds and precipitation and understanding global water and energy cycles. His research articles have appeared in major scientific journals.

Dr. Shin is a member of the American Meteorological Society and the American Geophysical Union.

Kenneth P. Bowman received the B.S. degree in environmental design from the University of Colorado, Boulder, in 1979 and the Ph.D. degree in geophysical fluid dynamics from Princeton University, Princeton, NJ, in 1984.

He was a National Research Council Resident Research Associate with the National Aeronautics and Space Administration Goddard Space Flight Center, Greenbelt, MD, from 1983 to 1985. Following this, he was an Assistant Professor with the University of Illinois, Urbana. He is currently with Texas A&M University, College Station, where he was first an Associate Professor then a Professor and, since 2007, has been the Head of the Atmospheric Sciences Department. His textbook An Introduction to Programming with IDL (Amsterdam; Academic Press, 2006) is used in a variety of science and engineering fields. He has published papers in the areas of climate dynamics, stratospheric ozone, and atmospheric dynamics, with an emphasis on the large-scale transport of trace substances.

Dr. Bowman is a member of the American Geophysical Union and American Meteorological Society.

Jung-Moon Yoo received the B.S. degree in meteorology from Yonsei University, Seoul, Korea, and the Ph.D. degree from the University of Maryland, College Park, in 1990, concentrating on the air–sea interaction of freshwater budget.

From 1986 to 1991, he was with the Climate and Radiation Branch, National Aeronautics and Space Administration (NASA) Goddard Space Flight Center, Greenbelt, MD, where he used data from the Infrared Interferometer Spectrometer to detect cirrus cloud. He is currently a Professor with the Ewha Womans University, Seoul, Korea, where he has taught since 1991. He has also been a NASA Visiting Scientist since then, contributing to the analyses of global warming and rain retrieval problems from satellite microwave data.

Long S. Chiu (SM'06) was born 1953 in Hong Kong. He received the B.S. degree in physics from the University of Miami, Coral Gables, 1974, and the Sc.D. degree in meteorology from the Massachusetts Institute of Technology, Cambridge, in 1980.

He is currently a Professor at the Institute of Space and Earth Information Science, Chinese University of Hong Kong, Hong Kong. He is a tenured Associate Professor (2001–present) and was a Research Professor (1998–2000) at George Mason University, Fairfax VA, a Senior Scientist and Group Manager (1989–1998) at SAIC/General Sciences Corporation, a Contract Scientist at the NASA Goddard Space Flight Center, and a Visiting Scholar at Center for Space and Remote Sensing Research, National Central University, Taiwan (1992). His current research interests include microwave remote sensing, rainfall estimation and analysis, climate change and variability, and aerosol–cloud–precipitation interactions.

Prof. Chiu is a Fellow of the Electromagnetics Academy, a member of the American Meteorological Society, American Geophysical Union, Sigma Xi, Sigma Pi Sigma, past president (2004–2006) of the Chinese-American Ocean-Atmosphere Association, and President (2007–2009) of the Hong Kong Society of Photogrammetry and Remote Sensing.